

Magnetic Fields in Superconducting Thin Films, Verification by Muon Spin Rotation

Nathan Abraham

November 29, 2011

Abstract

Magnetic fields in a superconducting film are modeled by a vortex lattice. The formulation of Pearl for a single vortex in a semi-infinite bulk superconductor is extended to a thin film. The field distribution for an array of vortices is obtained by summing the fields from the individual vortices. Numerical methods are used to calculate field distribution and obtain the rms of field variation σ_b which provides a measure of superconducting electron density. Muon spin rotation, μ SR, is explored as a technique to study the magnetic field distributions in the superconducting films.

1 Introduction

Muon spin rotation (μ SR) allows local magnetic fields to be probed in superconducting materials. In Niedermayer et al.[2] a low energy μ^+ beam allowed fields near the surface of a film to be studied. In that case the film thickness was on the order of but larger than penetration depth λ . Here we calculate fields for thinner films with a thickness closer to λ . High quality, single crystal superconductors can be obtained as thin films grown on a substrate.

2 Calculations

We expand upon the calculations of the Pearl geometry in which the superconducting region fills the half space $z > 0$ to one in which a film is centered on $z = 0$ by applying appropriate boundary conditions. The Ginzburg-Landau equation:

$$\frac{-\nabla^2 \mathbf{A}}{\mu_0} = \mathbf{J}_s = \frac{e^2}{m} [-A |\psi|^2 - (\frac{i\phi_0}{4\pi})(\psi^* \nabla \psi - \psi \nabla \psi^*)] \quad (1)$$

gives the vector potential inside the superconducting region for a single vortex as:

$$\nabla \times \nabla \times \mathbf{A} + (1/\lambda^2)\mathbf{A} = \frac{\phi_0 \hat{\theta}}{2\pi\lambda^2 r} \quad (2)$$

Where $\phi_0 = 2.07 \times 10^3$ gauss \cdot kÅ is the flux quantum. Outside the superconducting region \mathbf{A} is expressed by

$$\nabla \times \nabla \times \mathbf{A} = 0 \quad (3)$$

Using cylindrical coordinates and centering the z axis on the vortex, \mathbf{A} can be written as $\mathbf{A} = \hat{\theta}f(r, z)$. Then (2) and (3) become

$$\frac{\partial^2 f_2}{\partial z^2} + \frac{\partial}{\partial r} \frac{1}{r} \frac{\partial}{\partial r} r f_2 - \frac{1}{\lambda^2} f_2 = -\frac{\phi_0}{2\pi\lambda^2 r} \quad (4)$$

and

$$\frac{\partial^2 f_1}{\partial z^2} + \frac{\partial}{\partial r} \frac{1}{r} \frac{\partial}{\partial r} r f_1 = 0 \quad (5)$$

respectively.

In the Pearl geometry the solution inside the metal becomes:

$$f_2 = \int_0^\infty \frac{\phi_0}{2\pi\lambda^2} \frac{J_1(\gamma r)}{\gamma^2 + 1/\lambda^2} \left[1 - \frac{\gamma \exp(-(\gamma^2 + 1/\lambda^2)^{1/2} z)}{\gamma + (\gamma^2 + 1/\lambda^2)^{1/2}} \right] d\gamma \quad z > 0 \quad (6)$$

Let $s = (\gamma^2 + 1/\lambda^2)^{1/2}$, then we can write (6) as:

$$f_2 = \int_0^\infty \frac{\phi_0}{2\pi\lambda^2} \frac{J_1(\gamma r)}{s^2} \left[1 - \frac{\gamma \exp(-sz)}{\gamma + s} \right] d\gamma \quad (7)$$

And the solution outside

$$f_1 = \int_0^\infty \frac{\phi_0}{2\pi\lambda^2} \frac{J_1(\gamma r)}{s^2} e^{\gamma z} \frac{s}{s + \gamma} d\gamma \quad z < 0 \quad (8)$$

For a film of thickness d, centered on the $z = 0$ plane, the solution inside is:

$$f_2 = \int_0^\infty \frac{\phi_0}{2\pi\lambda^2} \frac{J_1(\gamma r)}{s^2} \left[1 - \frac{\gamma [\exp(-s(z + d/2)) + \exp(+s(z - d/2))]}{s(1 - e^{-sd}) + \gamma(1 + e^{-sd})} \right] d\gamma \quad (9)$$

Outside the solution becomes:

$$f_1 = \begin{cases} \int_0^\infty \frac{\phi_0}{2\pi\lambda^2} \frac{J_1(\gamma r)}{s^2} \frac{(1 - e^{-sd}) e^{-\gamma(z - d/2)} s}{s(1 - e^{-sd}) + (1 + e^{-sd}) \gamma} d\gamma & \text{if } z > d/2 \\ \int_0^\infty \frac{\phi_0}{2\pi\lambda^2} \frac{J_1(\gamma r)}{s^2} \frac{(1 - e^{-sd}) e^{\gamma(z + d/2)} s}{s(1 - e^{-sd}) + (1 + e^{-sd}) \gamma} d\gamma & \text{if } z < -d/2 \end{cases} \quad (10)$$

3 Results

3.1 Fields

The field lines for a single vortex are plotted for two films of varying thickness in figure (1). In both cases a significant radial component occurs away from the

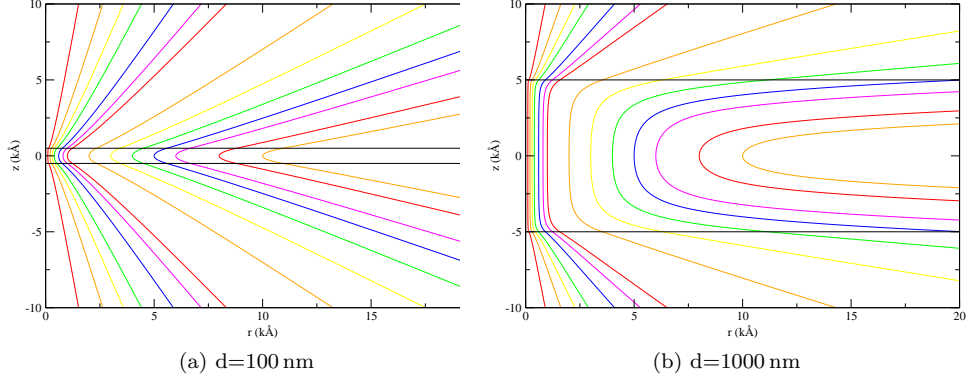


Figure 1: Field lines for 1.0 kÅ and 10 kÅ films with a penetration depth $\lambda = 1.3$ kÅ.

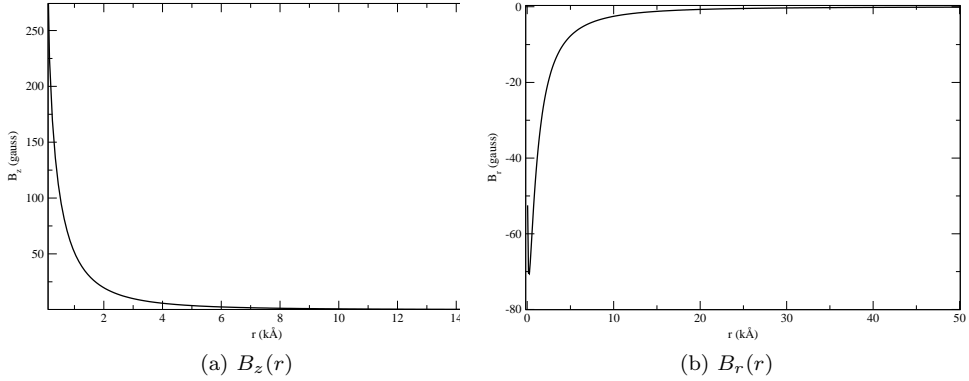


Figure 2: $B_z(r, z)$ and $B_r(r, z)$ plotted near the edge of a 1.0 kÅ film. $\lambda = 1.3$ kÅ.

vortex core and near the surface; near the core and deep in the metal it drops significantly.

Figure (2) shows the local field components for a single vortex. The perpendicular and radial components are plotted as a function of r for points near the film's lower surface. Both drop off fairly sharply as one moves away from the vortex. B_z appears sharper, which seems to agree with figure (1) where B_r becomes more dominant further from the core.

The magnetic flux is calculated for a single vortex. Figure (3a) plots flux within a 10 kÅ radius as a function of film thickness for various penetration depths. For large radii, calculated flux approaches the flux quantum $\phi_0 = 2.07 \times 10^3$ (kÅ)². Near the vortex flux is reduced for smaller thicknesses. A consequence of reduced flux close to the vortex would be a reduced σ_b which could be measured.

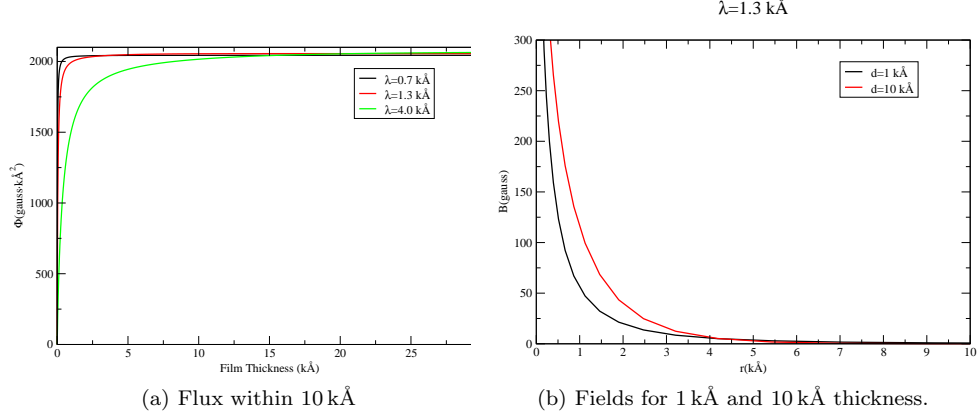


Figure 3: Flux for a single vortex. Figure(3a) Shows flux taken at midplane within a 10 kÅ radius of the vortex versus thickness for various λ . Figure(3b) shows fields calculated at the edge of 1 kÅ and 10 kÅ samples for $\lambda = 1.3 \text{ kÅ}$

Figure (3b) shows the z component of fields for a single vortex calculated at center of films of 1 kÅ and 10 kÅ thickness. The total flux for the thinner film appears smaller, however they converge for large r .

The second moment is plotted as a function of film thickness in figure (4a) for a penetration depth of 1 kÅ . σ_b drops off sharply for $d < \lambda$. Figure (4b) show second moment as a function of temperature. The values are obtained by varying λ in the calculation by the relation:

$$\lambda^2(T) = \lambda^2(0)\sqrt{1 - (T/T_c)^2} \quad (11)$$

Where $\lambda(0) = \lambda_0$ is the experimentally determined zero temperature penetration depth. The second moment is related to $\lambda(T)$ by:

$$\sigma_b \propto \frac{\lambda_0^2}{\lambda^2(T)} \quad (12)$$

3.2 μSR

The field distribution for an array of vortices is calculated by summing fields of individual vortices in a two dimensional equilateral triangle lattice. μSR is explored as a technique to experimentally determine behavior of magnetic fields in thin films. Simulated data is generated for both parallel and transverse polarized beams in various regions of a characteristic section of the triangular lattice. The applied magnetic field is perpendicular to the film for both cases. In the transverse case the initial polarization of the muon beam is perpendicular to the applied field; in the parallel case it is parallel. Figure (5a) shows polarization as a function of time $P(t)$ in the x direction for muons initially polarized as such.

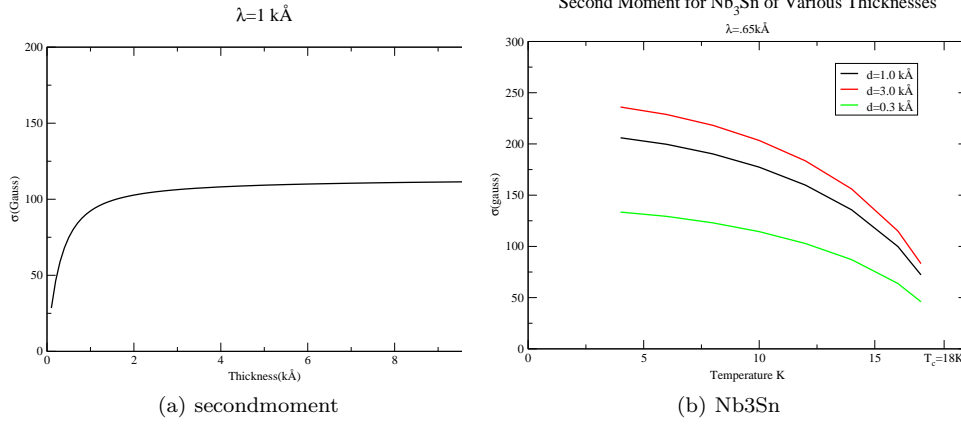


Figure 4: Second moments calculated for various temperatures and thicknesses. Figure (4a) plot σ_b as a function of thickness for $\lambda = 1 \text{ kÅ}$. Figure(4b) shows σ_b as a function of temperature where $\lambda_0 = .65 \text{ kÅ}$.

$P(t)$ is averaged over two separate slices of film, one near the edge and one close to the center. Similarly figure(5b) plots $P(t)$ for muons polarized parallel to the applied magnetic field and measured in the same direction.

4 Numerical Methods

The ffc and hv programs are used to calculate magnetic fields for an array of vortices. The ffc program calculates fields inside the film for 17 layers inside the film out to a radius of approximately 44 kÅ for a single vortex. The output is then read in by hv which calculates fields on a characteristic section of the lattice for an array of vortices. The z component average and rms is computed for each layer and the sum of layers.

d and λ are read in as input and vector potential inside the film is computed similarly to equation (9). The argument of the integral is summed over $\gamma = .01/r$ to 100 with double precision variables. J_1 is computed with a polynomial fit of the bessel function.

$$arz(r, z, d, \lambda) = \sum_{\gamma=.01/r}^{100} \frac{\phi_0}{2\pi\lambda^2} \frac{J_1(\gamma r)}{s^2} \left[1 - \frac{\gamma[\exp(-s(z+d/2)) + \exp(+s(z-d/2))]}{s(1-e^{-sd}) + \gamma(1+e^{-sd})} \right] \quad (13)$$

A partial derivative method is used to calculate magnetic fields. The radial component $B_r = -\frac{\partial f_2}{\partial z}$ is computed as

$$hrrz(r, z, d, \lambda) = \frac{-(arz(r, z + .005, d, \lambda) - arz(r, z - .005, d, \lambda))}{.01} \quad (14)$$

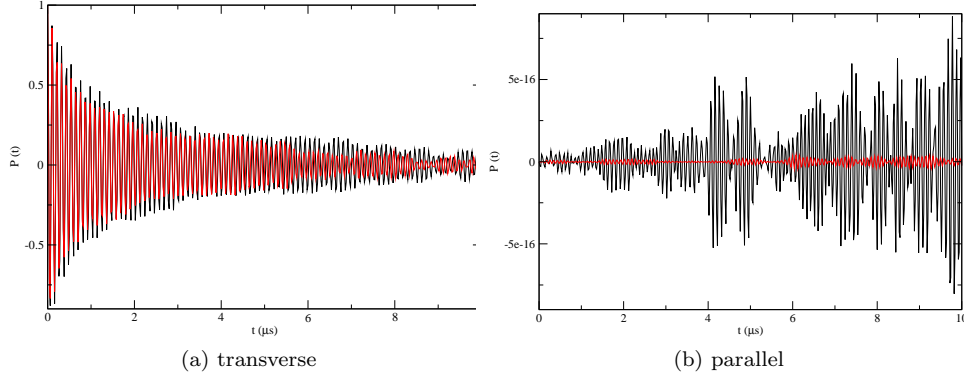


Figure 5: Simulated μ SR data for transverse and parallel field. Black: Muons stopping near film surface. Red: Muons stopping in center of film. The parallel polarized muon have nearly zero amplitude

The component parallel to the vortex core $B_z = \frac{1}{r} \frac{\partial}{\partial r} (r f_2)$ is computed as

$$h_z r z(r, z, d, \lambda) = \frac{(r + .005) a r z(r + .005, z, d, \lambda) - (r - .005) a r z(r - .005, z, d, \lambda)}{.01 * r} \quad (15)$$

The fields are calculated for a range of (r_i, z_k) , $r_i = .01 \cdot 1.3^i$ for $i : 0 \rightarrow 32$ for each layer and $z_k = k \cdot d/17$ for $k : 0 \rightarrow 8$. Symmetry allows the layers on both sides of the $z = 0$ plane to be calculated simultaneously. The components for each r and z are listed in two data files to be read in by hv.

Fields are calculated for an array of vortices with spacing of $a = 1.546 \text{ k}\text{\AA}$ in an equilateral triangle configuration corresponding to a perpendicular 1k Gauss field. The set of vortices calculated over is shown in figure (6).

A characteristic region for field calculations is chosen as a right triangle with a vertex at the origin vortex, one at the midpoint towards the vortex along the x axis, and one at the centroid of the lattice triangle. See figure (7a). The region is divided into 40×40 grid with $\Delta x \approx 19.82 \text{ \AA}$ and $\Delta y \approx 11.44 \text{ \AA}$. B_x, B_y , and B_z components the field for each point within the closure of the region are calculated for each vortex by linear interpolation between r_i data points read in from ffc and summed with the singularity at the origin excluded. The process is repeated for each z_k layer.

Average field for each layer is determined by a weighted sum. There is a singularity at the origin so this index is excluded. The 90 deg corner is weighted $\frac{1}{4}$ th of the interior. The other vertex is weighted $\frac{1}{8}$ and the second index along the bottom next to the origin is weighted $\frac{3}{8}$. The edge indices are weighted $\frac{1}{2}$ and the second line of indices in along the hypotenuse are weighted $\frac{7}{8}$. The rms of field is calculated for each layer and averaged over the layers with middle layer given a weight of $\frac{1}{2}$.

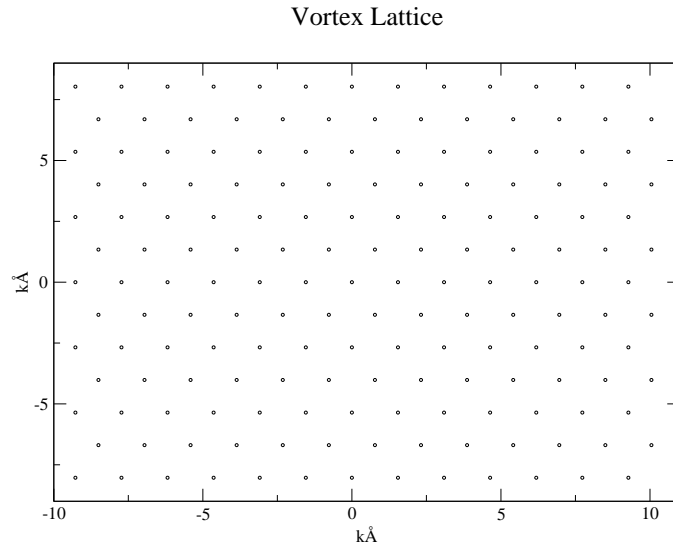


Figure 6: Vorticities used to calculate fields. There is one at the origin and six in each direction of the lattice axes.

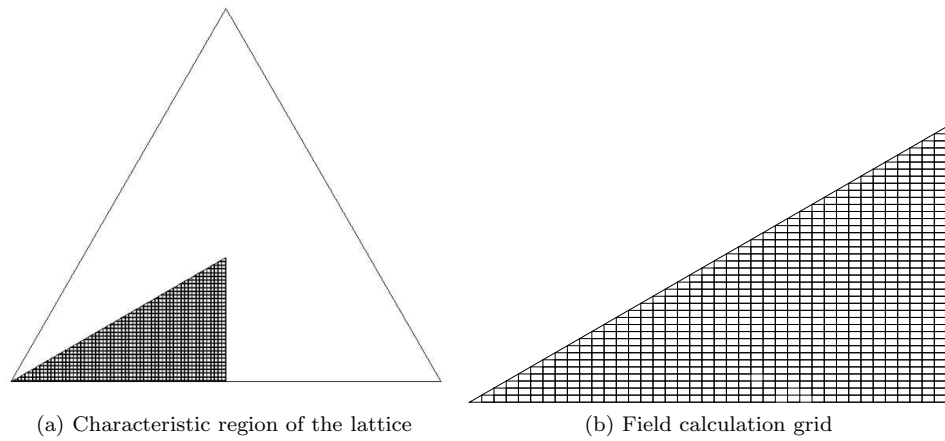


Figure 7: Region of the lattice where fields are calculated. Figure(7a) shows the calculated region within a lattice triangle. The left vertex is the origin vortex. Figure (7b) shows the points where the field is calculated. The boundaries are included but must be partially weighted.

5 Conclusion

Experimentation could be used to evaluate these methods on thin films. Second moment dependence on thickness could be used to extend experimental data on thin films to obtain superconducting electron density for larger geometries. These calculations will need to be extended to include coherence length ξ for samples with large cores such as Nb.

References

- [1] Ch. Niedermayer, E.M. Forgan, H. Glücker, A. Hofer, E. Morenzoni, M. Pleines, T. Prokscha, T.M. Riseman, M. Birke, T.J. Jackson, J. Litterst, M.W. Long, H. Luetkens, A. Schatz, and G. Schatz. Direct Observation of a Flux Line Lattice Field Distribution across an $YBa_2Cu_3O_{7-\delta}$ surface by Low Energy Muons. *Physical Review Letters*, 83(19):3932–3935, 1999.
- [2] Judea Pearl. Structure of Superconductive Vortices near a Metal-Air Interface. *Journal of Applied Physics*, 37(11):4139–4141, 1966.